Korean J. Chem. Eng., **29**(8), 1094-1101 (2012)
DOI: 10.1007/s11814-011-0284-1

A novel synthesis of spherical $LiFePO_4$/C composite using $Fe_{1.5}P$ and mixed lithium salts via oxygen permeation

Guixin Wang, Rui Liu, Miao Chen, Hanchang Kang, Xiuli Li, and Kangping Yan†

College of Chemical Engineering, Sichuan University, Chengdu 610065, China
(*Received 13 July 2011 • accepted 6 November 2011*)

Abstract–A novel route was designed to synthesize $LiFePO_4$/C composites by using the $Fe_{1.5}P$ byproduct, mixed lithium salts, and permeated oxygen from air via a rheological phase method. The reaction process was investigated with various techniques. When the calcining time was increased from 10 to 30 h, the gradual formation of olivine structure was observed. The growth kinetics of the crystals was analyzed. SEM and TEM results indicated the as-synthesized $LiFePO_4$ was constituted of small spheres covered with carbon particles. The discharge capacity of the $LiFePO_4$/C composite prepared at ~700 °C for ~25 h could reach 139.7 mAh g^{-1} and still remained 130.2 mAh g^{-1} after 15 cycles at 0.2 C rate, comparable to that of the reported $LiFePO_4$/C composite using conventional methods. Cyclic voltammogram confirmed the $LiFePO_4$/C composite had a high purity and good lithium ion insertion/desertion redox behavior.

Key words: $LiFePO_4$/C Composite, $Fe_{1.5}P$ Byproduct, Rheological Phase Method, Thermal Analysis, Electrochemical Performance

INTRODUCTION

Energy and environmental issues are becoming more and more important nowadays, with clean energy materials attracting increasing attention due to the scarcity and the environmental impact of traditional fossil fuel resources. Advanced lithium-ion batteries and/or supercapacitors, for example, have been suggested as potential energy carriers for transportation applications. $LiMPO_4$ (M denotes transition metals like Fe, Mn, Ni) is a group of promising, green and low cost alternative electrode materials for lithium-ion batteries or supercapacitors in comparison with the commercial electrode material $LiCoO_2$ [1-3]. Currently, $LiFePO_4$ has become a focus from fundamental to applications. To overcome the disadvantage of poor inherent electronic conductivity, various carbon sources [4-6] or metal phosphides formed by carbon reduction during the synthesis process [2,5-7] are utilized. The synthesis is usually carried out under an inert atmosphere like Ar or N_2 via the reduction of the oxides of Fe or P by carbon or hydrogen. As a result, high cost (especially when using Fe^{2+} salt or $FePO_4$) and environmental pollution hinder the extensive application of $LiFePO_4$ in the field of electric vehicles or standby power sources. It is essential to exploit novel raw materials or reaction routes to synthesize $LiFePO_4$ with low cost.

As an intermetallic compound, the elements of Fe and P mix well in a Fe-P alloy, so it is possible to synthesize $LiFePO_4$ using Fe-P alloy. Because Fe-P alloy has no element oxygen, the reaction to synthesize $LiFePO_4$ using Fe-P alloy needs some oxygen to take part in the oxidization of P, which is different completely from the current methods using absolute reductive atmosphere for preparing $LiFePO_4$ [8,9]. On the other hand, Fe-P alloy can be obtained in large quantities as the byproduct from thermal processes for producing phosphorus [8]. To afford satisfactory electrochemical performance, electrode materials with specific morphology such as 3D pore, core-shell, or spheres have been applied and show interesting properties [4,10-13]. Some usual methods for preparing spherical materials include sol-gel process [4], ball-milling-assisted reaction [10], hydrothermal synthesis [11], co-precipitation [12], and ultrasonic spray pyrolysis [13]. By combining the advantages of solid-state reaction and liquid phase reaction, a rheological phase method is a process for synthesizing functional materials by dispersing solid powders uniformly in a liquid phase using proper amount of solvents like water, ethanol, or benzene. In a rheological mixture, the close contact between the solid particles and the liquid, along with the enhanced heat exchange and ion transfer, affords a preferred condition to favorably utilize the surface area of particles and to accurately control the reaction temperature [14-18]. In addition, ceramic membrane technology has been adopted to provide oxygen effectively from air [19-21].

In this study, $LiFePO_4$/C composites were synthesized by calcining the rheological phase precursor composed of Fe-P byproduct, combined lithium salts and $NH_4H_2PO_4$ as complement P source. The required oxygen was provided by the permeation of air through a corundum ceramic crucible wall. The detailed reaction process, influence of the calcining time, formation mechanism, and electrochemical performance were investigated.

EXPERIMENTAL SECTION

1. Preparation

$LiFePO_4$/C composites were prepared via a rheological phase method by using ethanol as a dispersing agent, and the flow chart is shown in Fig. 1. The Fe-P alloy, a byproduct from the electrothermal reduction process for producing yellow phosphorus, was pulverized and ground finely to simultaneously provide elements of Fe and P for $LiFePO_4$. By combining the results from X-ray diffraction (XRD) and inductively coupled plasma-atomic emission

†To whom correspondence should be addressed.
E-mail: yankp@scu.edu.cn

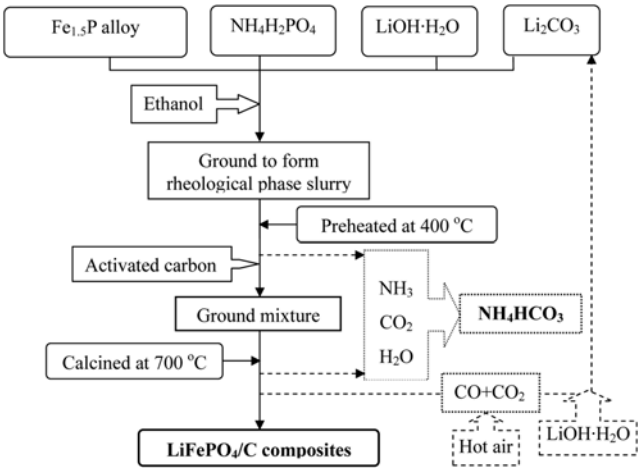

Fig. 1. Flow chart for preparing $LiFePO_4$/C composites using $Fe_{1.5}P$ alloy.

spectrometry (ICP-AES), the compositional formula of the Fe-P alloy was determined $Fe_{1.5}P$ [22]. Thus, a novel reaction route was designed as follows by adopting mixed lithium sources of Li_2CO_3 and $LiOH{\cdot}H_2O$ to adjust the molar ratio of the by-produced NH_3 and CO_2 so as to synthesize the valuable fertilizer NH_4HCO_3.

$$2Fe_{1.5}P+Li_2CO_3+LiOH{\cdot}H_2O+NH_4H_2PO_4+4O_2 \longrightarrow 3LiFePO_4+NH_3\uparrow+CO_2\uparrow+3H_2O\uparrow \quad (1)$$

Powders of $Fe_{1.5}P$ (~98.0%), Li_2CO_3 (~99.6%), $LiOH{\cdot}H_2O$ (~99.2%), and $NH_4H_2PO_4$ (~99.0%) were stoichiometrically weighted and thoroughly ground with ethanol solution in an agate mortar to form the first rheological phase precursor. Small amount of carbon could be added to make the initial product loose. Then the as-obtained precursor was transferred to a corundum ceramic crucible without cap and preheated at ~400 °C for 4-7 h in a muffle oven under air. After being cooled to ambient temperature, the preheated precursor was mixed with mesopore activated carbon with a high BET surface area (~2,000 $m^2\ g^{-1}$) in an ethanol solution to form the second rheological phase precursor. Carbon was added to confine the growth of the product grain and act as the carbon source for the products. In the meantime, the added carbon can react with the permeated oxygen from air to prevent the oxidization of Fe^{2+} in the product. Finally, the second precursor was overlaid with more carbon black and transferred to a capped corundum ceramic crucible to be further calcined at ~700 °C in a muffle oven for various lengths of calcining time to obtain different products. The carbon black was placed on top of the preheated precursor to provide a protective atmosphere for Fe^{2+} during the calcining process because carbon can react with the remnant and permeated oxygen in the capped crucible. Such carbon black was removed when the product was cooled to room temperature. Thus, the carbon content in the final product can be controlled effectively by adjusting the initial added carbon content and the permeated oxygen via the selection of corundum ceramic crucible.

2. Characterization

XRD was utilized to investigate the structure and the phase purity of the raw material, precursor and products at various stages. From 15 to 70°, XRD was recorded on a Philips X'Pert Pro diffractometer with a step of 2°/min using Cu Kα radiation at a power of 40 kV ×100 mA. To discuss the reaction process, thermal analysis was performed from ~40 to ~1,000 °C at a ramp rate of 10 °C/min under air on a NETZSCH STA 449C instrument. The morphology and the particle size were observed by using scanning electron microscopy (SEM, JEOL JSM-5900LV, Japan) and transmission electron microscopy (TEM, JEOL JEM100CX II, Japan). The particles on the surface of products were analyzed by energy dispersion spectrum (EDS). The carbon content in the product was measured by the weight difference before and after the product in a hot HCl solution (~18.5 wt%). $LiFePO_4$ is dissolved in such solution while the carbon is insoluble. After being filtrated and rinsed with a dilute HCl solution (~1.85 wt%) and high purity water (~17.6 MΩ·cm), the insoluble substance was dried at ~110 °C and weighed to give the carbon content in the product.

The electrochemical performance was evaluated using 2032 coin cells via galvanostatic charge/discharge tests and cyclic voltammetry. The as-synthesized $LiFePO_4$/C composite powders were ground and then mixed well with 15 wt% of conductive acetylene black and 5 wt% of commercial LA-132 binder (Chengdu Indigo Power Sources Co. Ltd., China). The mixture was then mechanically homogenized in an agate mortar to form an even slurry for coating on a cleaned aluminum foil. After being dried at 100 °C under vacuum for at least 10 hours, the foil was laminated and cut into 1.2 cm^2 wafers for use as working electrodes. Metal lithium was utilized as both the counter electrode and the reference electrode [22,23]. In an argon-filled glove box, 2032 cells were assembled by sandwiching a Celgard 2300 microporous separator between two electrodes using an electrolyte of a 1.0 M $LiPF_6$ dissolved in a solution of ethylene carbonate (EC), dimethyl carbonate (DMC) and ethyl methyl carbonate (EMC) (1 : 1 : 1 in vol, Shenzhen Capchem Chemicals Co. Ltd., China). The above cells were tested galvanostatically between 2.4 and 4.2 V *vs.* Li^+/Li at room temperature on a Neware battery-testing instrument (Shenzhen Neware Technology Ltd., China). Cyclic voltammetry (CV) was performed on a PAR273A potentiostat/galvanostat (Princeton Applied Research, USA).

RESULTS AND DISCUSSION

1. Reaction Design

Different from current reports on the synthesis of $LiFePO_4$, which eliminates oxygen to provide an absolute non-oxidative atmosphere [1-7], oxygen is required as a reactant for the oxidation of P in the $Fe_{1.5}P$ alloy, as shown in reaction (1). However, extra oxygen will oxidize the Fe^{2+} in the $LiFePO_4$ product to Fe^{3+}. Therefore, it is vital to control the amount of oxygen from air for reaction (1) in order to avoid the oxidation of Fe^{2+} ions simultaneously during the synthesis process. The crucible is composed of corundum ceramic which allows permeation of oxygen [19-21]. So it is possible for the oxygen from air to enter the inner side of the crucible to take part in reaction, which has been demonstrated in the control experiment performed in an air-tightness quartz glass tube. In the control experiment, a large quantity of FeP, Fe_2P and little $LiFePO_4$ with poor crystalline remained in the product when the second precursor was calcined under identical reaction conditions, indicating that the element P in the $Fe_{1.5}P$ raw material was not oxidized completely because of absent oxygen.

The bond energies of C-O in CO, P-O in PO_4^{3-}, C-O in CO_2, and Fe-O in Fe_2O_3 are 1075.0, 596.6, 532.2, and 409.0 kJ mol^{-1} [24], respectively. Furthermore, PO_4^{3-} has a Lewis structure of tetrahedron and the P exhibits resonance as there is a double bond with one oxygen atom and three single bonds with other three oxygen atoms, so PO_4^{3-} is stable enough to be reduced hardly by carbon below ~800 °C [2-7]. The permeated oxygen through the corundum ceramic membrane of the crucible would oxidize the P in the unreacted Fe-P alloy in the preheated precursor to form stable P-O bonds when the second precursor was calcined at ~700 °C, and then more permeated oxygen would be consumed by the carbon in the second precursor. The mechanism for the protective atmosphere formed from the carbon at the surface of the second precursor is as follows: the carbon reacts first with the remnant oxygen from air in the upper chamber of the capped corundum ceramic crucible to produce CO_2:

$$C+O_2 \longrightarrow CO_2\uparrow,\ \Delta H_r^o=393.5\ kJ\cdot mol^{-1} \quad (2)$$

That leaves an inert atmosphere of nitrogen in the upper chamber of the capped crucible. Simultaneously, the produced CO_2 will further react with the carbon at the gas/solid interface of CO_2 and carbon to form CO by using the discharge heat of the reaction (2):

$$C+CO_2 \longrightarrow 2CO\uparrow,\ \Delta H_r^o=-172.5\ kJ\cdot mol^{-1} \quad (3)$$

The produced CO can mix with the residual N_2 in the upper chamber of the crucible to form a protective atmosphere because of their similar mass densities. Additionally, the amount of oxygen declines gradually with the thickening of the carbon layer in the crucible, and small amount of oxygen may react with the carbon at high temperature to produce CO directly.

$$2C+O_2 \longrightarrow 2CO\uparrow,\ \Delta H_r^o=221.0\ kJ\cdot mol^{-1} \quad (4)$$

The mixed gases of reductive CO and inert N_2 construct a multiple protective atmosphere in the upper chamber of the crucible. Thus, the oxygen from air becomes difficult to access the bottom materials in the crucible crossing through the upper carbon layer to oxidize element P. Therefore, the required oxygen is only obtained through the permeation of air to the inner side of the crucible through the corundum ceramic membrane wall, and the oxygen amount can be controlled by the selection of crucible and the added carbon in the second precursor.

The by-produced CO gas during the synthesis process could be introduced into a reaction chamber full of hot air to form CO_2 which is further adsorbed by a solution of LiOH to prepare Li_2CO_3 raw materials, and the expressions are as follows:

$$2CO+O_2 \longrightarrow 2CO_2\uparrow,\ \Delta H_r^o=566.0\ kJ\cdot mol^{-1} \quad (5)$$

$$CO_2+2LiOH \longrightarrow Li_2CO_3+H_2O \quad (6)$$

According to reaction (1), mixed lithium salts were used to produce NH_3 and CO_2 in a molar ratio of 1 : 1. NH_3, which originated from the decomposition of $NH_4H_2PO_4$ at below 250 °C, was introduced into cold water to form $NH_3\cdot H_2O$ first. Then, the by-produced CO_2 at higher temperature was introduced into the above $NH_3\cdot H_2O$ to form the valuable NH_4HCO_3 solution, while the cooling heat was recycled to heat up the precursor, by the reaction of

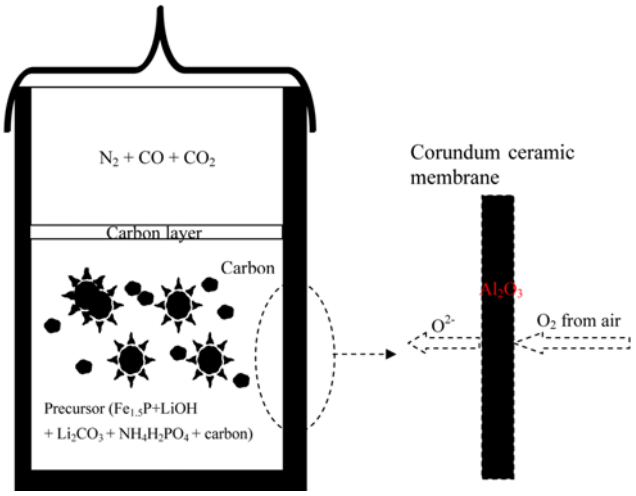

Fig. 2. Possible mechanism for the oxygen control.

$$NH_3+H_2O+CO_2 \xrightarrow{-30\ ^\circ C} NH_4HCO_3 \quad (7)$$

Consequently, a novel route was designed to synthesize $LiFePO_4$ by using $Fe_{1.5}P$ byproduct as the elemental sources of Fe and partial P. The oxygen from air was used as the oxidant. Carbon added to the preheated precursor was expected to confine the grain growth and to control the consumption of oxygen for synthesizing $LiFePO_4$. The required oxygen amount can be controlled successfully via the balance between the permeation through the corundum ceramic membrane of the crucible and the consumption by the carbon in the precursor; the possible mechanism is provided in Fig. 2. The permeated oxygen amount and the consumed oxygen amount can be adjusted by the type of the ceramic crucible and the initial added carbon amount to the preheated precursor, respectively.

2. Precursor Analysis

The XRD patterns of the $Fe_{1.5}P$ raw material, preheated precursor, and final product obtained by calcining the second precursor at ~700 °C for 25 h are summarized in Fig. 3. According to the XRD analysis results using Rietveld refinement, the $Fe_{1.5}P$ was composed of orthorhombic FeP (JPCDS card number 78-1443) and hexago-

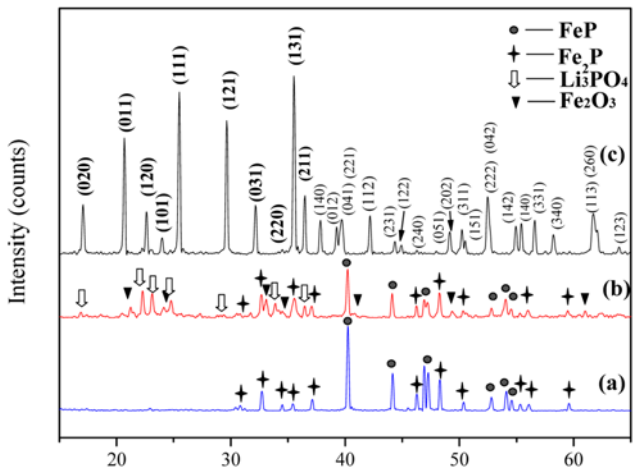

Fig. 3. XRD patterns of $Fe_{1.5}P$ (a), preheated precursor (b), and product obtained by calcining for ~25 h (c).

nal Fe_2P (JPCDS card number 01-1200). In the preheated precursor calcined at ~400 °C in air, there were obvious indexed peaks of FeP, Fe_2P, Li_3PO_4 (JPCDS card number 12-0230) and Fe_2O_3 (JPCDS card number 02-0919), without indexed peaks of Li_2CO_3, $LiOH{\cdot}H_2O$, $NH_4H_2PO_4$ or LiH_2PO_4, indicating the raw materials of Li_2CO_3, $LiOH{\cdot}H_2O$ and $NH_4H_2PO_4$ were reacted and part of the $Fe_{1.5}P$ raw material was oxidized during the preheating process, which is further confirmed by the thermal analysis later. New phase of Li_3PO_4 shows that $NH_4H_2PO_4$ did not react with Li_2CO_3 or $LiOH{\cdot}H_2O$ to form LiH_2PO_4, and Fe_2O_3 originated from the oxidization of $Fe_{1.5}P$ alloy. In addition, the peak intensities of the FeP and Fe_2P in the $Fe_{1.5}P$ raw material are much stronger than those of the corresponding phases in the preheated precursor under the same conditions, suggesting that the $Fe_{1.5}P$ raw material was partially reacted. When the preheated precursor mixed and covered with carbon was further calcined at ~700 °C for 25 h in the capped corundum ceramic crucible, a black product with clear crystal structure was obtained. The indexed peaks of the product match well with those of the standard pattern of $LiFePO_4$ (JPCDS card number 40-1499), indicating that the product is olivine $LiFePO_4$ with an orthorhombic structure and a Pmnb space group. A detailed analysis of the $LiFePO_4$ product will be given later. The fact from the raw material to the product demonstrates the designed novel reaction (1) and the corresponding technics are possible to prepare $LiFePO_4$ using $Fe_{1.5}P$ alloy and oxygen from air.

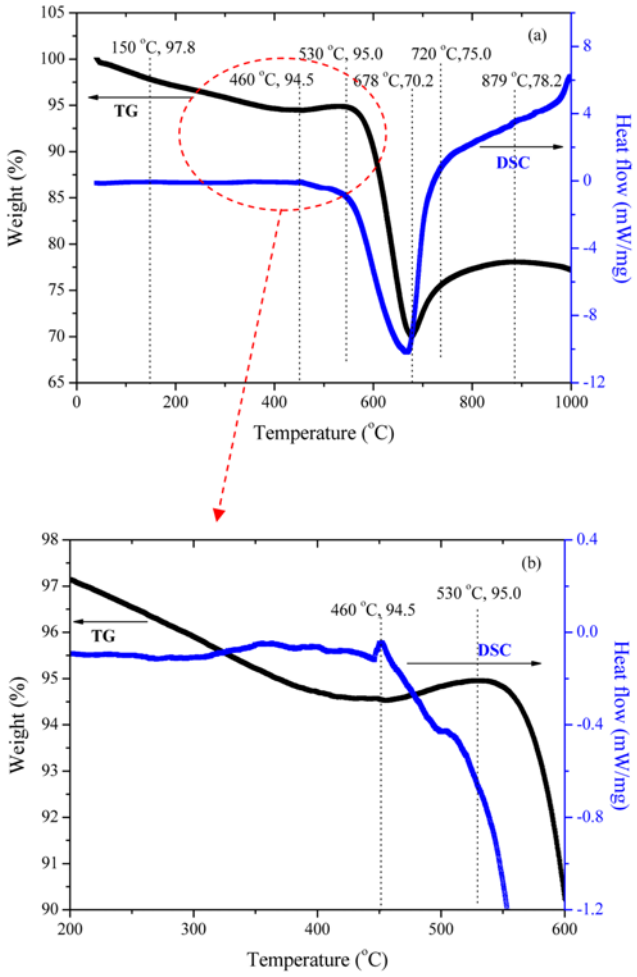

Fig. 4. Thermal analysis of the precursor whole (a), and part (b).

3. TG-DSC Analysis

To investigate the detailed reaction process, thermodynamic analysis was conducted in air with a heating rate of 10 °C/min. The simultaneous thermogravity (TG) and differential scanning calorimetry (DSC) plots of the precursor, including stoichiometric mixtures of $Fe_{1.5}P$, $LiOH{\cdot}H_2O$, Li_2CO_3 and $NH_4H_2PO_4$, are shown in Fig. 4. To understand the thermal property clearly, a part amplified thermal analysis curve during the temperature ranging from ~200 to ~600 °C is provided in Fig. 4(b). There are several stages of weight loss and gain in the TG plot and both endothermic and exothermic peaks in the DSC plot. When the temperature increases from ~40 to ~150 °C, there is an initial weight loss of ~2.2 wt% and a small endothermic peak, corresponding to the evaporation of physically adsorbed water and ethanol in the precursor and the dehydration reaction of the $LiOH{\cdot}H_2O$ [5]:

$$LiOH{\cdot}HO_2 \longrightarrow LiOH+H_2O \quad (8)$$

When the temperature reaches ~460 °C, the continuous weight loss is ~3.3 wt%, while there is a small endothermic peak. The decomposition temperature of $NH_4H_2PO_4$ ranges from 160 to 230 °C, and the theoretic weight loss of the produced NH_3 from the $NH_4H_2PO_4$ is ~2.5 wt% by considering the carbon in the precursor. The produced H_3PO_4 from the $NH_4H_2PO_4$ will further react with LiOH and Li_2CO_3 to form Li_3PO_4 and lose partial water or CO_2. Additionally, the reactions between H_3PO_4 and mixed lithium salts of LiOH and Li_2CO_3 are exothermic because of the acid-alkali neutralization reaction, corresponding to the exothermic peak in the DSC curve at ~460 °C. Therefore, the weight loss of ~3.3 wt% is considered to come from the decomposition of $NH_4H_2PO_4$ and the removal of partial water or CO_2 from the reaction between the intermediate product H_3PO_4 and the mixed lithium salts. The decomposition reaction is as follows:

$$NH_4H_2PO_4 \longrightarrow H_3PO_4+NH_3\uparrow \quad (9)$$

According to the above preheated precursor analysis, the intermediate product is Li_3PO_4, and the whole reaction between the intermediate product H_3PO_4 and the mixed lithium salts of LiOH and Li_2CO_3 is as follows:

$$H_3PO_4+Li_2CO_3+LiOH \longrightarrow Li_3PO_4+CO_2\uparrow+2H_2O\uparrow \quad (10)$$

When the temperature ranges from ~460 to ~530 °C, there is a slight weight increase of ~0.5 wt% and a large quick endothermic peak in the DSC curve, which may originate from the partial oxidization of $Fe_{1.5}P$ in the precursor. XRD pattern in Fig. 3 confirms the oxidization behavior and there are obvious indexed peaks of Fe_2O_3 besides part of indexed peaks of FeP and Fe_2P in the preheated precursor. The reaction is as follows:

$$2Fe_{1.5}P+4.75O_2 \longrightarrow 1.5Fe_2O_3+P_2O_5 \quad (11)$$

Because P_2O_5 has a strong exothermic character when reacting with water, the produced P_2O_5 will react with H_2O to release heat, corresponding to the exothermic peak in the DSC curve at ~500 °C. The reaction has no weight change:

$$3H_2O+P_2O_5 \longrightarrow 2H_3PO_4 \quad (12)$$

As the temperature is increased to ~678 °C, there is a sharp weight loss of ~24.8 wt% and a large quick endothermic peak. When the temperature continuously reaches ~720 °C, there is a slight weight increase of ~4.8 wt% and an increased exothermic peak. The changes of weight and caloric may originate from the combined reactions of the oxidization of carbon in the precursor and the reaction to form $LiFePO_4$. The exothermic caloric from the oxidization of carbon can be used to produce $LiFePO_4$, and the reaction expressions are as follows:

$$C+O_2 \longrightarrow CO_2 \uparrow \quad (13)$$

$$C+CO_2 \longrightarrow 2CO \uparrow \quad (14)$$

$$1.5Fe_2O_3+2Fe_{1.5}P+2Li_3PO_4+2H_3PO_4+3.25O_2 \longrightarrow 6LiFePO_4+3H_2O \uparrow \quad (15)$$

When the temperature continuously increases from ~720 to ~879 °C, the increased weight and the exothermic peak are from the oxidization of Fe^{2+} in the $LiFePO_4$ product:

$$12LiFePO_4+3O_2 \longrightarrow 4Li_3Fe_2(PO_4)_3+2Fe_2O_3 \quad (16)$$

After ~879 °C, the weight loss is from the deoxidization of Fe_2O_3 at high temperature:

$$2Fe_2O_3 \longrightarrow 4FeO+O_2 \uparrow \quad (17)$$

As a result, proper oxygen amount is significant for the reaction to prepare olivine $LiFePO_4$ with clear crystal structure.

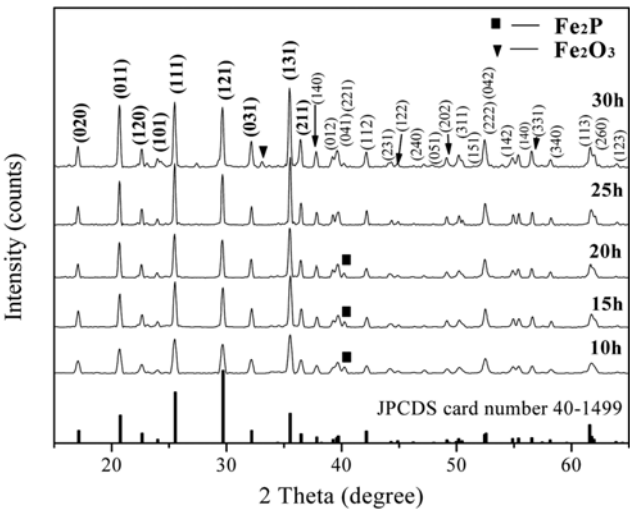

Fig. 5. XRD patterns of various $LiFePO_4$ products.

4. XRD Analysis

Fig. 5 shows the XRD patterns of various products obtained with different lengths of calcining time. All the products predominantly have a clear orthorhombic structure, and the main indexed peaks match well with the standard peaks of the $LiFePO_4$ (JPCDS card number 40-1499), indicating the products are mainly olivine $LiFePO_4$. Among the indexed peaks, four main peaks centered at $2\theta \approx 20.8^o$, 25.5^o, 29.7^o, and 35.5^o can be attributed to (011), (111), (121), and (131) planes of $LiFePO_4$, respectively [1-7]. Calculating from the peaks of the main planes using Scherrer's formula [17,23], the average crystalline size of the produced $LiFePO_4$ samples is summarized in Table 1. Simultaneously, the lattice parameters along the axes of a, b, c, along with the cell volume obtained using Rietveld refinement, are also compared in Table 1. With the calcining time prolonged from 10 to 30 h, the peak densities of the product become sharper, and the average crystalline size increases from 37.17 to 39.75 nm, obeying the crystal growth kinetics law. In spite of the different lengths of calcining time, the lattice parameters and cell volumes are close to those of the standard $LiFePO_4$. When the calcining time increases from 10 to 20 h, there is a weak peak of impurity phase at ~40.2° whose peak density declines gradually under the same conditions, thus the smooth diminishing of the impurity. According to the above XRD analysis and the references [3,4,6,7], the impurity phase can be attributed to Fe_2P which is from the incomplete reaction of $Fe_{1.5}P$ raw material during the short calcining time. When the calcining time reaches 25 h, the peak of impurity phase of Fe_2P disappears, suggesting the reaction is completed. However, when the calcining time reaches 30 h, there is another new weak peak of impurity phase at ~32.8° which can be assigned to Fe_2O_3 by comparing with the standard pattern in the JPCDS cards, indicating the product is partially oxidized.

The weight difference before and after dissolving the product in a hot HCl solution showed the carbon content in the product declined from ~30 to 0 wt% when the calcining time was prolonged from 10 to 30 h, indicating the carbon in the precursor took part in the reaction to consume more permeated oxygen with longer calcining time. As the calcining time reached ~25 h, the carbon content was ~9 wt% and there was no impurity peak of Fe_2P or Fe_2O_3 in the XRD pattern of the product, indicating no oxidization of Fe^{2+} when carbon was present. When the calcining time reached 30 h, the carbon content was ~0 wt% and there was a weak peak of impurity Fe_2O_3 in the XRD pattern of the product, indicating part of the Fe^{2+} in the $LiFePO_4$ product was oxidized by more permeated oxygen because the carbon in the precursor was consumed during the long calcining period.

Table 1. Lattice parameters and grain sizes of the as-synthesized $LiFePO_4$

Product	Lattice parameters			Grain volume ($Å^3$)	Average grain size (nm)
	a (Å)	b (Å)	c (Å)		
10 h	6.01	10.34	4.70	291.68	37.17
15 h	6.01	10.33	4.70	291.73	38.30
20 h	6.01	10.35	4.71	292.80	38.99
25 h	6.01	10.34	4.70	291.75	39.15
30 h	6.02	10.34	4.70	292.46	39.75
JPCDS card number 40-1499	6.02	10.35	4.70	292.95	-----

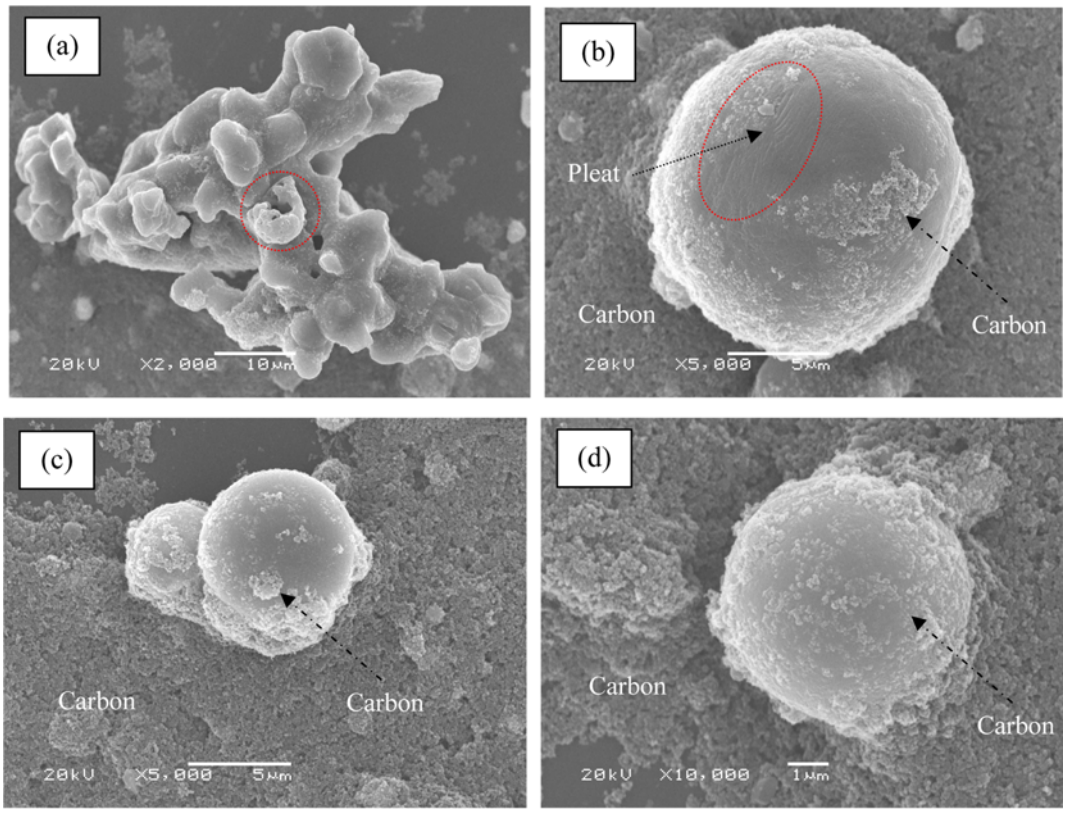

Fig. 6. SEM images of the as-synthesized $LiFePO_4$/C composite.

Thus, series of products obtained with different lengths of calcining time and thermal analysis demonstrate that it is possible to synthesize $LiFePO_4$ using $Fe_{1.5}P$ alloy and oxygen from air according to the designed novel reaction (1).

5. SEM and TEM Analysis

From the SEM images shown in Fig. 6, the product synthesized with calcining time of ~25 h is constituted of small $LiFePO_4$ spheres covered with carbon particles, which were confirmed by EDS analysis. Besides many dispersed small spheres, some spheres aggregate. According to the images of the collapsed part and the whole, the sphere is hollow with relatively smooth surface, instead of an aggregation of many small particles. The diameter of the spheres ranges from 4 to 9 μm, and the wall thickness is ~500 nm. There are some pleats on the surface of $LiFePO_4$, which may originate from the escaped H_2O gas produced in the inner of the sphere due to reaction (15). Spheres have a high accessible surface area and high active reaction sites for lithium ions insertion/extraction. Carbon in the product is beneficial for improving conductivity and to store electrolytes to make Li^+ ions move easily for enhancing the electrochemical performance of $LiFePO_4$ [4-6]. At the same time, pleats will increase the surface area and active sites for electrolyte storage and Li^+ ions reaction.

From the TEM images in Fig. 7, the as-synthesized $LiFePO_4$ with calcining time of ~25 h is composed of spherical particles with many

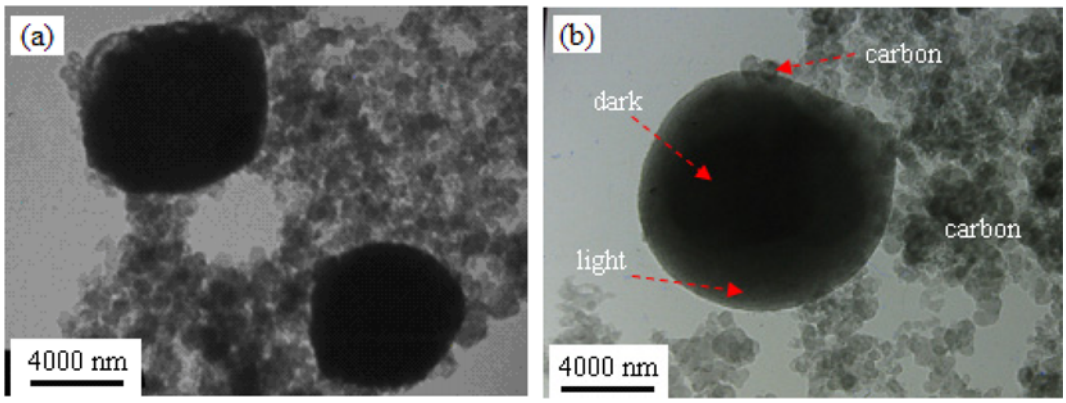

Fig. 7. TEM images of the as-synthesized $LiFePO_4$/C composite.

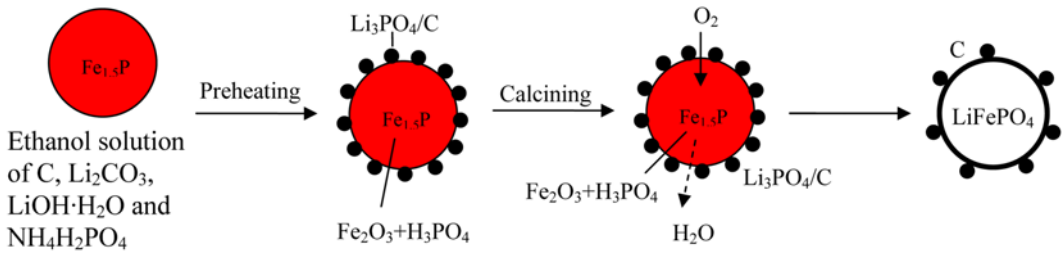

Fig. 8. Schematic illustration for the formation of hollow spherical $LiFePO_4$/C composite.

fragments and carbon particles. According to the EDS analysis, the dark particles are $LiFePO_4$ and the tint particles are carbon, which are due to the different lattice parameters [23,25]. Small carbon particles at the surface of $LiFePO_4$ spheres agree well with the above SEM results.

Based on the above analysis results, a possible formation mechanism for the hollow spherical product is supplied in Fig. 8. In the first rheological phase precursor, the added carbon will adsorb the ethanol solution of Li_2CO_3, $LiOH·H_2O$ and $NH_4H_2PO_4$, and cover the small $Fe_{1.5}P$ particles. After being preheated at low temperature of ~400 °C, the produced H_3PO_4 from $NH_4H_2PO_4$ reacts with LiOH and Li_2CO_3 to form Li_3PO_4 at the surface of the $Fe_{1.5}P$ particles, while part of the $Fe_{1.5}P$ is oxidized to Fe_2O_3 and P_2O_5 which will further react with the intermediate product of H_2O to form H_3PO_4. After being further calcined at high temperature of ~700 °C, the surrounded $Fe_{1.5}P$ particles react with the intermediate products of Fe_2O_3, H_3PO_4, and Li_3PO_4, as well as the permeated O_2 from air, to form spherical $LiFePO_4$. At the same time, more by-produced H_2O escapes to leave pleats at the $LiFePO_4$ surface and remove the carbon at the pleat area. Some remnant carbon covers the as-synthesized hollow spherical $LiFePO_4$ product to form $LiFePO_4$/C composite.

6. Electrochemical Performance

The typical galvanostatic charge/discharge curves and the initial cycle performance of the as-synthesized $LiFePO_4$/C composite with calcining time of ~25 h at a current rate of 0.2 C are shown in Fig. 9. The $LiFePO_4$/C composite had a steady charge platform at ~3.45 V that corresponds to the Li^+ extraction and a discharge platform at ~3.40 V that corresponds to the Li^+ insertion, agreeing well with the reports [1,4-6,12]. The median voltage difference between the charge plateau and the discharge plateau was 0.05 V, indicating the resistance was not large. The maximum discharge capacity and the corresponding coulombic efficiency obtained by dividing the discharge capacity by the charge capacity of the $LiFePO_4$/C composite could reach 139.7 mAh g^{-1} and 99.1%, respectively. After 15 cycles at 0.2 C, the discharge capacity still remained 130.2 mAh g^{-1}, about 93.2% of the maximum value. Furthermore, the fade tendency became slow during cycling process. Except one pair of redox peaks

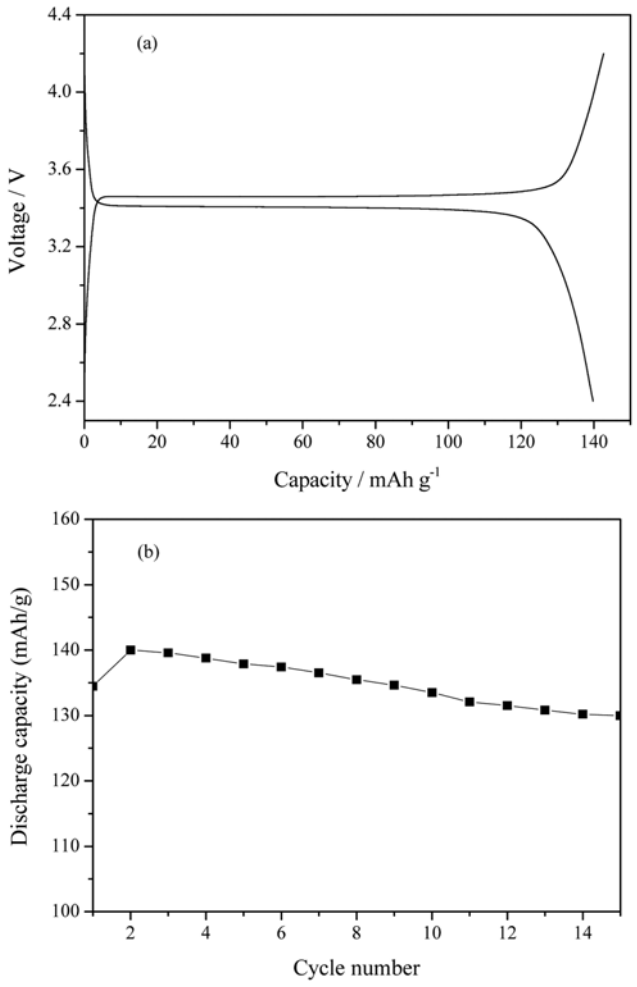

Fig. 9. Typical galvanostatic charge/discharge curves (a), and cycle performance (b) of the $LiFePO_4$/C composite at 0.2 C current rate.

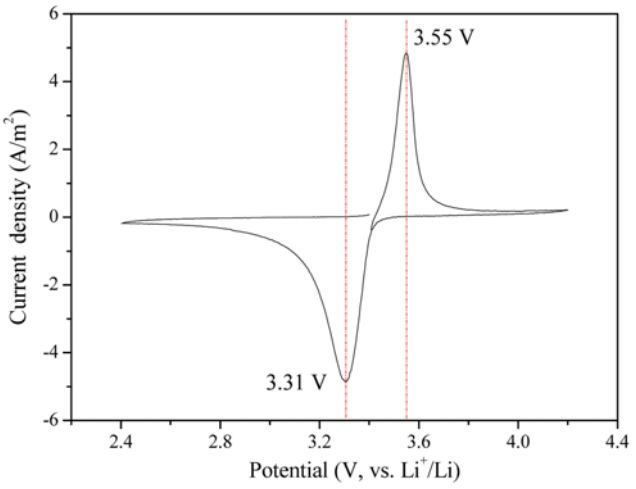

Fig. 10. Cyclic voltammogram of the $LiFePO_4$/C composite at a scan rate of 0.2 mV/s.

corresponding to $LiFePO_4$, the cyclic voltammogram in Fig. 10 had no other redox peaks, indicating that the $LiFePO_4$/C composite had a high purity and good redox behavior. The oxidization peak relating to Li^+ extraction and the reduction peak relating to Li^+ insertion were at ~3.55 and ~3.31 V, respectively. The redox peak positions were similar to the fine-structured $LiFePO_4$ synthesized using $LiCOOCH_3 \cdot 2H_2O$, $FeC_2O_4 \cdot 2H_2O$, $NH_4H_2PO_4$, and oleic acid [26]. The primary electrochemical performance was comparable with that of the reported $LiFePO_4$/C composite synthesized from $Fe(CH_3COO)_2$ or Fe_2O_3 and $NH_4H_2PO_4$ using conventional methods [1,4-6,12,25]. More electrochemical performances, such as more cycles, rate performance, carbon influence, particle size effect, impurity effect, cyclic voltammograms with various scan rates, and electrochemical impedance curves, are under investigation.

CONCLUSIONS

Series of $LiFePO_4$/C composites were prepared successfully using $Fe_{1.5}P$ byproduct and oxygen from air via a novel reaction route. The reaction process was investigated in detail. The results of thermal analysis indicated that $Fe_{1.5}P$ alloy was partially oxidized at first, and then reacted with Fe_2O_3, Li_3PO_4, H_3PO_4, and permeated oxygen from air to form $LiFePO_4$. XRD patterns confirmed the product obtained by calcining with 25 h was $LiFePO_4$ with good olivine structure and high purity. The carbon content was found to be ~9 wt% according to weight difference. SEM and TEM images demonstrated that the as-synthesized $LiFePO_4$ had a good hollow spherical morphology, and some carbon particles and small pleats were at the surface. The formation mechanism and the crystal growth kinetics of the products were discussed. The discharge capacity of the $LiFePO_4$/C composite could reach 139.7 mAh g^{-1} and still remained 130.2 mAh g^{-1} after cycling, comparable with those of the reported $LiFePO_4$/C composite synthesized using conventional method [1,4-6,12,25]. Cyclic voltammogram further showed high purity and good redox behavior. The initial experimental results are beneficial for exploiting novel reaction processes and cheap raw materials for producing $LiFePO_4$ at low cost.

ACKNOWLEDGEMENTS

This work is financially supported by Youth Foundation of Sichuan University (07046). Assistance from the Analytical & Testing Center of Sichuan University is greatly acknowledged. We thank Prof. Bin Wang for an insightful discussion.

REFERENCES

1. A. K. Padhi, K. S. Nanjundaswamy and J. B. Coodenough, *J. Electrochem. Soc.*, **144**, 1188 (1997).
2. P. S. Herle, B. Ellis, N. Coombs and L. F. Nazar, *Nature Mater.*, **3**, 147 (2004).
3. Y. R. Wang, Y. F. Chen, S. Q. Cheng and L. N. He, *Korean J. Chem. Eng.*, **28**, 964 (2011).
4. J. L. Li, T. Suzukib, K. Naga, Y. Ohzawa and T. Nakajima, *Mater. Sci. Eng. B*, **142**, 86 (2007).
5. Y. B. Xu, Y. J. Lu, L. Yan, Z. Y. Yang and R. D. Yang, *J. Power Sources*, **160**, 570 (2006).
6. Z. Y. Chen, H. L. Zhu, S. Ji, R. Fakir and V. Linkov, *Solid State Ionics*, **179**, 1810 (2008).
7. C. W. Kim, J. S. Park and K. S. Le, *J. Power Sources*, **163**, 144 (2006).
8. G. X. Wang and K. P. Yan, China Patent, 200,810,045,243.1 (2008).
9. R. Liu, G. X. Wang, K. P. Yan and X. L. Li, *Chin. J. Syn. Chem.*, **18**, 639 (2010).
10. G. X. Wang, J. J. Xu, M. Wen, R. Ca, R. Ran and Z. P. Shao. *Solid State Ionics*, **179**, 946 (2008).
11. J. J. Chen, M. J. Vacchio, S. J. Wang, N. Chernova, P. Y. Zavalij and M. S. Whittingham, *Solid State Ionics*, **178**, 1676 (2008).
12. G. H. Kim, S. T. Myung, H. S. Kim and Y. K. Sun, *Electrochim. Acta*, **51**, 2447 (2006).
13. V. Jokanovic, A. M. Spasic and D. Uskokovic, *J. Colloid Interface Sci.*, **278**, 342 (2004).
14. G. X. Wang, B. L. Zhang, Z. L. Yu and M. Z. Qu, *Solid State Ion.*, **176**, 1169 (2005).
15. Y. G. Liang, S. J. Yang, Z. H. Yi, X. F. Lei, J. T. Sun and Y. H. Zhou, *Mater. Sci. Eng. B*, **121**, 152 (2005).
16. W. J. Zhou, S. J. Bao, B. L. He, Y. Y. Liang and H. L. Li, *Electrochim. Acta*, **51**, 4701 (2006).
17. J. Jiang, L. C. Li, F. Xu and Y. L. Xie, *Mater. Sci. Eng. B*, **137**, 166 (2007).
18. H. Liu, Y. Feng, K. Wang and J. Y. Xie, *J. Phys. Chem. Solids*, **69**, 2037 (2008).
19. C. H. Liao, *Bull. Chin. Ceram. Soc.*, **3**, 56 (2004).
20. A. H. Heuer, *J. Eur. Ceram. Soc.*, **28**, 1495 (2008).
21. I. Ganesh, G. J. Reddy, G. Sundararajan, S. M. Olhero, P. M. C. Torres and J. M. F. Ferreira, *Ceram. Int.*, **36**, 473 (2010).
22. M. Zhao, G. X. Wang, X. L. Li, F. Wang, R. Liu and K. P. Yan, *Met. Mater. Int.*, **16**, 993 (2010).
23. G. X. Wang, K. P. Yan, Z. L. Yu and M. Z. Qu, *J. Appl. Electrochem.*, **40**, 821 (2010).
24. J. A. Dean, *Lange's Chemistry Handbook* (15th Ed.), McGraw-Hill, New York (1999).
25. S. T. Myung, S. Komaba, N. Hirosaki, H. Yashiro and N. Kumagai, *Electrochim. Acta*, **49**, 4213 (2004).
26. D. Choi, D. Wang, V. V. Viswanathan, I. T. Bae, W. Wang, Z. Nie, J. G. Zhang, G. L. Graff, J. Liu, Z. Yang and T. Duong, *Electrochem. Commun.*, **12**, 378 (2010).